

# Reachability and Region of Attraction Analysis Applied to GTM Dynamic Flight Envelope Assessment

Rohit Pandita\*, Peter Seiler†  
and Gary Balas‡

The objective of the NASA Aviation Safety Program is to improve the safety of current and future aircraft operating in the National Airspace System. Research under this program has focused on vehicle design, construction, operation and maintenance. Reducing aircraft loss of control accidents is critical to increasing aviation safety as it is the largest and most fatal aircraft accident category. Loss of control accidents result in aircraft operation outside the normal flight envelope in regions where aerodynamic data is either poorly characterized or unavailable. Hence it is important to monitor, in real-time, aircraft states and environmental conditions to assess the current state of the aircraft flight envelope. This paper describes the development of algorithms for dynamic flight envelope assessment using reachable set and nonlinear region of attraction techniques and their application to the NASA Generic Transport Model (GTM). The ability to estimate a safe envelope around various operating trim points is demonstrated.

## Nomenclature

$I_{zz}$	Principal moment of inertia about Z-axis [lb-ft <sup>2</sup> ]
$b$	Wing span [ft]
$\bar{c}$	Mean chord [ft]
$S_{ref}$	Wing reference area [ft <sup>2</sup> ]
$C_x, C_z, C_m$	X,Z body axes force and pitching moment coefficients [nondimensional]
$\bar{q}$	Dynamic pressure [lb/ft <sup>2</sup> ]
$\Delta X, \Delta Y, \Delta Z$	Displacement between cartesian coordinates of two points [ft]
$m$	Mass [slugs]
$g$	Acceleration due to gravity [ft/s <sup>2</sup> ]
$\omega_{\frac{b}{2U}}$	Normalized steady state component of body angular velocity [rad/s]
$q$	Pitch rate, body axis [rad/s]
$\hat{q}$	Normalized Pitch rate, body axis [rad/s]
$EAS, U$	Equivalent Air Speed [ft/s]
$\theta$	Pitch attitude [rad]
$\varepsilon$	radian-to-degree, $180.0/\pi$
$\alpha$	Angle of attack [rad]
$LUT$	Look up table
$\delta_e$	Elevator control surface deflection [rad]
$\delta_{th}$	Throttle position, normalized [0 – 1]

## I. Introduction

Flight safety is recognized as of paramount importance and extensive research has been carried out especially over the last two decades with strong support from all stakeholders, the industry, government agencies

---

\*Graduate Student, Department of Aerospace Engineering and Mechanics, Student Member AIAA

†Senior Research Associate, Department of Aerospace Engineering and Mechanics

‡Professor and Head, Department of Aerospace and Engineering and Mechanics, Associate Fellow AIAA

responsible for flight safety and the academia.<sup>1</sup> Numerous commercial aircraft accidents in the past were found to be caused by exceeding the aircraft flight envelope, in many of which the flight crew was unaware of it. The safe flight envelope of an airplane may change over a period of service life due to aging of airframe, degradation of flight control system (FCS) elements, engines, etc. Hence constant assessment of the aircraft flight envelope is important for safety of flight.

An aircraft flight envelope is defined as the range of airspeed, altitudes and normal load factors at which the aircraft can operate safely. All automatic flight control systems contain a flight envelope protection or limiting system to improve the safety of the vehicle. Note that the flight envelope is dependent on the aircraft dynamics. Dynamic assessment of the flight envelope, in real-time, is important to keeping the pilots, as well as the flight control system informed of the current controllability, aircraft state and structural limits of the aircraft. We are investigating the use of reachable set and nonlinear region of attraction techniques for dynamic flight envelope assessment as part of the NASA Fault Diagnosis, Prognosis and Reliable Flight Envelope Assessment (FDP-FEA) NRA. The program objective is to provide real-time dynamic flight envelope information to the pilot and on-line adaptation of the flight control system to maintain stability and safe flight during normal and failure conditions. A multi-discipline technical approach to flight envelope assessment is taken which draws on new results from system identification, fault diagnosis and prognosis to identify the aircraft states and anomalies in flight. A combination of on-line and off-line information is used to generate the dynamic achievable flight envelope which includes structural limits, controllability, and current state of the aircraft. Calculation of the achievable flight envelope requires approximation of the nonlinear aircraft dynamics by a linear, parameter-varying model and solution of a convex optimization.

Two complementary approaches are taken in this paper to flight envelope assessment. The first exploits controllability and reachability properties of linear systems to address flight envelope assessment. This same underlying theory has been successfully applied to the optimal control problem decades ago. In order to extend the results to the nonlinear airplane dynamics problem, extension of the results for linear models have been proposed, e.g. to piecewise linear models and linear parameter varying (LPV) models. For example Shin<sup>2</sup> has applied the theory of reachable sets for linear parameter varying (LPV) systems, Cross and Mitchell<sup>3</sup> have applied level set methods using the Hamilton-Jacobi partial differential equation (HJPDE). Bayen and Tomlin<sup>4</sup> have applied the HJPDE to a hybrid system for autoland maneuver safety analysis. On the other hand, nonlinear methods based on Lyapunov's stability theory have been proposed<sup>5-9</sup> and applied successfully as a region of attraction (ROA) prediction tool. ROA methods offer the ability to predict a stable set in state space around a given equilibrium in which the system will return to the equilibrium. An application scenario could be an aircraft trimmed for cruise flight experiencing an upset condition due to an atmospheric phenomenon like gust, windshear, turbulence, etc. It is vitally important to know if such an upset condition could potentially destabilize the aircraft without a chance of recovery.

It is clear that reachability analysis and ROA methods complement each other nicely. Reachability analysis allows us to predict to some extent the states that can be reached with a given control authority from a trim condition, this knowledge is useful from outer loop guidance perspective as it can be used as safety advisory for the flight crew or hard constraints for guidance and trajectory optimization algorithm onboard such that aircraft is not attempted to be driven to states beyond the reach of its control authority. To complement this, ROA methods can be used to analyze if a future intended trim point generated by the guidance algorithm onboard has a large enough safety envelope around it to protect against upset conditions. In this paper these complementary approaches are applied to the NASA Generic Transport Model (GTM) to showcase how these methods can be applied to improve flight safety.

## A. Paper Organization

The paper is organized in the following manner. First, the underlying theory of reachable sets for linear systems and nonlinear region-of-attraction (ROA) is presented. Next, the derivation of the longitudinal axis polynomial model of the GTM aircraft is presented. The longitudinal axis polynomial model is compared with the full nonlinear model through time-domain simulation for validation. A simple pitch angle tracking controller is presented and applied to the GTM aircraft in section B. Section IV presents results on reachable sets and ROA analysis obtained for the GTM aircraft. For the analysis, a nominal straight and level trim flight condition of EAS= 150ft/s is used throughout the paper.

## II. Tools for dynamic flight envelope assessment

The state of the aircraft plays an important role in assessing if flight envelope constraints and specifications are being satisfied. For linear systems, the controllability and observability of the system is directly related to the reachable set of states. We are using reachable set analysis techniques to aid in dynamic flight envelope assessment for aircraft.<sup>2</sup> The combination of the reachable set and conventional flight envelope is called achievable state envelope for a given bounded energy and bounded magnitude inputs in the presence of flight anomalies. Calculation of the reachable set for linear systems can be posed as a linear matrix inequality. In general though, calculation of the reachable set for a nonlinear system is a nontrivial task. It is a time consuming process to calculate the boundary of a reachable set in the state space. Hence we have initially focused on calculation of reachable sets for nominal and damaged linearized aircraft models. For calculation of the reachable sets for nonlinear aircraft models, the nonlinear aircraft will be represented as a linear, parameter-varying (LPV) system and LPV reachable set techniques will be applied.

### A. Linear analysis: Reachability

A linear time invariant (LTI) dynamical system is given by,

$$\begin{aligned}\dot{x}(t) &= Ax(t) + Bu(t) \\ y(t) &= Cx(t) + Du(t)\end{aligned}\tag{1}$$

where,  $x \in \mathbb{R}^n$ ,  $u \in \mathbb{R}^m$  and  $y \in \mathbb{R}^p$  are the states, inputs and outputs of the LTI system. The state of the system at time  $t_f$  can be determined by a state transition map,  $s(t_i, t_f, x_i, u(.))$  such that,

$$x(t_f) = s(t_f, t_i, x(t_i), u(.))\tag{2}$$

**Lemma 1** *Without loss of generality, let the origin be the equilibrium state of the system given in Eq.1. The dynamical system is said to be controllable on  $[t_0, t_1]$  if  $\forall$  initial states  $x_0 = x(t_0)$ ,  $\exists u(.) \in \mathcal{U}$  so that  $s(t_1, t_0, x(t_0), u(.)) = 0$ .*

**Lemma 2** *The dynamical system is said to be reachable on  $[t_0, t_1]$  if  $\forall$  final state  $x_1 = x(t_1)$ ,  $\exists u(.) \in \mathcal{U}$  so that  $s(t_1, t_0, x(t_0), u(.)) = x_1$ .*

In general, controllability does not imply reachability, but vice-versa is true.<sup>10</sup>

#### 1. Reachable sets with unit-energy inputs

The reachable set of states with unit input energy for the dynamical system given in Eq.1, denoted  $\mathcal{R}_{ue}$ , is defined as,

$$\mathcal{R}_{ue} = x(T) : \int_0^T u^T u dt \leq 1, T \geq 0.\tag{3}$$

Reachable sets can be bound by hyper-ellipsoids of the form,

$$\Gamma = \{\xi \mid \xi Q^{-1} \xi \leq 1\}$$

where,  $Q > 0$ . It can be shown<sup>11</sup> that for LTI systems ellipsoidal bounds can be computed by solving the following LMI feasibility conditions,

$$Q > 0, \begin{bmatrix} QA^T + AQ & B \\ B^T & -I \end{bmatrix} \leq 0\tag{4}$$

## 2. Reachable sets with unit-peak inputs

The reachable set of states with unit peak inputs for the dynamical system given in Eq.1,  $\mathcal{R}_{up}$  is defined as,

$$\mathcal{R}_{up} = \{x(T) : u^T u \leq 1, T \geq 0\}. \quad (5)$$

In Boyd, et al.<sup>11</sup> it is shown that this reachable set can be computed by solving the following LMI feasibility problem,

$$Q > 0, \alpha \geq 0, \begin{bmatrix} QA^T + AQ + \alpha Q & B \\ B^T & -\alpha I \end{bmatrix} \leq 0 \quad (6)$$

It shall be noted that LMI in Eq.6 is in fact a bilinear matrix inequality (BMI) since both  $\alpha$  and  $Q$  are unknowns. An optimal solution to a BMI is not easy to find and usually a bisection type algorithm is required to find a suboptimal solution. In Zheng, et al.<sup>12</sup> algorithms are presented to address this issue. Additionally, LMI problems in Eqs.4 and 6 can be cast as optimization problems by adding a cost function to be minimized. Since the objective is to find the minimum reachable set, the volume of the reachable ellipsoid can be minimized over which the given LMIs hold true. An easier approach is to use a cost function, such that the maximum diameter of the reachable ellipsoid in any coordinate, to be minimized. This problem can be cast easily as an eigenvalue problem (EVP),

$$\min \lambda, \quad s.t. \quad Q - \lambda I \leq 0, Q > 0 \quad (7)$$

While reachable sets with unit-input energy is significant to the problem of optimal control. From the perspective of dynamic flight envelope assessment (FEA) it can be argued that reachable sets with unit-peak input are of greater relevance.

## B. Region of attraction Analysis for nonlinear systems

Linear analysis is a local analysis which is only valid near the operating point. Many systems, including the GTM aircraft, are more accurately described by nonlinear dynamical systems. For linear systems asymptotic stability of an equilibrium point is a global property. In other words, if the equilibrium point is asymptotically stable then the state trajectory will converge back to the equilibrium when starting from any initial condition. A key difference with nonlinear systems is that equilibrium points may only be locally asymptotically stable. Khalil<sup>13</sup> and Vidyasagar<sup>14</sup> provide good introductory discussions of this issue. The region-of-attraction (ROA) of an asymptotically stable equilibrium point is the set of initial conditions whose state trajectories converge back to the equilibrium.<sup>13</sup> If the ROA is small, then a disturbance can easily drive the system out of the ROA and the system will then fail to come back to the stable equilibrium point. Thus the size of the ROA is a measure of the stability properties of a nonlinear system around an equilibrium point. This provides the motivation to estimate the region-of-attraction (ROA) for an equilibrium point of a nonlinear system. In this section we describe our technical approach to estimating the ROA.

Consider autonomous nonlinear dynamical systems of the form:

$$\dot{x}(t) = f(x(t)), \quad x(0) = x_0 \quad (8)$$

where  $x(t) \in \mathbb{R}^n$  is the state vector at time  $t$ . We assume that  $x = 0$  is a locally asymptotically stable equilibrium point. Formally, the ROA is defined as:

$$R_0 = \left\{ x_0 \in \mathbb{R}^n : \text{If } x(0) = x_0 \text{ then } \lim_{t \rightarrow \infty} x(t) = 0 \right\} \quad (9)$$

Computing the exact ROA for nonlinear dynamical systems is, in general, a very difficult problem. There has been significant research devoted to estimating invariant subsets of the ROA.<sup>5-7,15-20</sup> Our approach is to restrict the search to ellipsoidal approximations of the ROA. The ellipsoid is specified by  $\{x_0^T N x_0 \leq \beta\}$  where  $N = N^T > 0$  is a user-specified matrix which determines the shape of the ellipsoid. Given  $N$ , the problem is to find the largest ellipsoid contained in the ROA:

$$\begin{aligned} \beta^* &= \max \beta \\ \text{subject to: } &\{x_0^T N x_0 \leq \beta\} \subset R_0 \end{aligned} \quad (10)$$

Determining the best ellipsoidal approximation to the ROA is still a challenging computational problem. Instead we will attempt to solve for upper and lower bounds satisfying  $\underline{\beta} \leq \beta^* \leq \bar{\beta}$ . If these upper and lower bounds are close then we have approximately solved the best ellipsoidal approximation problem given in Equation 10.

The upper bounds are computed via a search for initial conditions leading to divergent trajectories. If  $\lim_{t \rightarrow \infty} x(t) = +\infty$  when starting from  $x(0) = x_{0,div}$  then  $x_{0,div} \notin R_0$ . If we define  $\bar{\beta}_{div} := x_{0,div}^T N x_{0,div}$  then  $\{x_0^T N x_0 \leq \bar{\beta}_{div}\} \not\subset R_0$ . Thus  $\bar{\beta}_{div}$  is a true upper bound on  $\beta^*$  and  $\{x_0^T N x_0 \leq \bar{\beta}_{div}\}$  is an outer approximation of the best ellipsoidal approximation to the ROA. An exhaustive Monte Carlo search is used to find the tightest possible upper bound on  $\beta^*$ . Specifically, initial conditions are randomly chosen starting on the boundary of a large ellipsoid: Choose  $x_0$  satisfying  $x_0^T N x_0 = g$  where  $g$  is sufficiently large that  $g \gg \beta^*$ . If a divergent trajectory is found, then an upper bound  $\bar{\beta}_{div}$  on  $\beta^*$  is computed by finding the minimum value of  $p$  along the divergent trajectory. The state vector  $x_{div}$  that achieves  $p(x_{div}) = \bar{\beta}_{div}$  is stored and  $g$  is decreased by a small factor, e.g.  $g = 0.995 \bar{\beta}_{div}$ . The search continues until a maximum number of simulations is reached.  $\bar{\beta}_{MC}$  will denote the smallest upper bound computed with this Monte Carlo search.

The lower bounds are computed using Lyapunov functions and recent results connecting sums-of-squares polynomials to semidefinite programming. To compute these bounds we need to further assume that the vector field  $f(x)$  in the system dynamics (Equation 8) is a polynomial function. The computational algorithm is briefly described in the following paragraphs. Additional details are provided in literature references.<sup>8, 21–27</sup> Lemma 3 is the main Lyapunov theorem used to compute lower bounds on  $\beta^*$ . This specific lemma is proved by Tan<sup>25</sup> but very similar results are given in textbooks, e.g. by Vidyasagar.<sup>14</sup>

**Lemma 3** *If there exists a continuously differentiable function  $V : \mathbb{R}^n \rightarrow \mathbb{R}$  such that:*

- $V(0) = 0$  and  $V(x) > 0$  for all  $x \neq 0$
- $\Omega_\gamma := \{x \in \mathbb{R}^n : V(x) \leq \gamma\}$  is bounded.
- $\Omega_\gamma \subset \{x \in \mathbb{R}^n : \nabla V(x)f(x) < 0\}$

then for all  $x \in \Omega_\gamma$ , the solution of Equation 8 exists, satisfies  $x(t) \in \Omega_\gamma$  for all  $t \geq 0$ , and  $\Omega_\gamma \subset R_0$ .

A function  $V$  satisfying the conditions in Lemma 3 is a Lyapunov function and  $\Omega_\gamma$  provides an estimate of the region of attraction. Any subset of  $\Omega_\gamma$  is also inside the ROA. In principle we can compute a lower bound on  $\beta^*$  by solving the maximization:

$$\begin{aligned} \underline{\beta} &:= \max \beta \\ \text{subject to: } &\{x_0^T N x_0 \leq \beta\} \subset \Omega_\gamma \end{aligned} \tag{11}$$

Our computational algorithm replaces the set containment constraint with a sufficient condition involving non-negative functions:

$$\begin{aligned} \underline{\beta} &:= \max \beta \\ \text{subject to: } &s(x) \geq 0 \quad \forall x \\ &-(\beta - x^T N x)s(x) + (\gamma - V(x)) \geq 0 \quad \forall x \end{aligned} \tag{12}$$

The function  $s(x)$ , known as a “multiplier” function, is a decision variable of the optimization, i.e. it will be found as part of the optimization. It is straight-forward to show that the two non-negativity conditions in Optimization 12 are a sufficient condition for the set containment condition in Optimization 11. If both  $V(x)$  and  $s(x)$  are restricted to be polynomials then both constraints involve the non-negativity of polynomial functions. A sufficient condition for a generic multi-variate polynomial  $p(x)$  to be non-negative is the existence of polynomials  $\{g_1, \dots, g_n\}$  such that  $p = g_1^2 + \dots + g_n^2$ . A polynomial which can be decomposed in this way is appropriately called a sum-of-squares (SOS). Finally, if we replace the non-negativity conditions in Optimization 12 with SOS constraints, then we arrive at an SOS optimization problem:

$$\begin{aligned} \underline{\beta} := \max \beta \\ \text{subject to: } s(x) \text{ is SOS} \\ -(\beta - x^T Nx)s(x) + (\gamma - V(x)) \text{ is SOS} \end{aligned} \tag{13}$$

It is sufficient to note that there are connections between SOS polynomials and semidefinite matrices. Moreover, optimization problems involving SOS constraints can be converted and solved as a semidefinite programming optimization. There is freely available software to set up and solve these problems.<sup>28–30</sup>

The choice of the Lyapunov function which satisfies the conditions of Lemma 3 has a significant impact on the quality of the lower bound,  $\underline{\beta}$ . The simplest method is to find  $P > 0$  which solves the Lyapunov equation  $A^T P + PA = -I$ .  $A := \left. \frac{\partial f}{\partial x} \right|_{x=0}$  is the linearization of the dynamics about the origin.  $V_{LIN}(x) := x^T Px$  is a quadratic Lyapunov function since  $x = 0$  is assumed to be a locally asymptotically stable equilibrium point. Thus we can solve for the largest value of  $\gamma$  satisfying the set containment condition in Lemma 3:  $\Omega_\gamma \subset \{x \in \mathbb{R}^n : \nabla V_{LIN}(x)f(x) < 0\}$ . This problem can also be turned into an SOS optimization with “multiplier” functions as decision variables.  $\underline{\beta}_{LIN}$  will denote the lower bound obtained using the quadratic Lyapunov function obtained from linearized analysis.

Unfortunately,  $\underline{\beta}_{LIN}$  is typically orders of magnitude smaller than the upper bound  $\bar{\beta}_{MC}$ . Several methods to compute better Lyapunov functions exist, including  $V$ - $s$  iterations,<sup>21–24</sup> bilinear optimization,<sup>25</sup> and use of simulation data.<sup>8,26,27</sup> We briefly describe the  $V$ - $s$  iteration starting from  $V_{LIN}$ . In the first step of the iteration, the multiplier functions and  $\underline{\beta}_{LIN}$  are computed. Then the multiplier functions are held fixed and the Lyapunov function candidate becomes the decision variable. The SOS constraints of this new problem are those which arise from the two set containment conditions:  $\Omega_\gamma \subset \{x \in \mathbb{R}^n : \nabla V_{LIN}(x)f(x) < 0\}$  and  $\{x_0^T Nx_0 \leq \beta\} \subset \Omega_\gamma$ . In the next iteration, the multiplier functions are again decision variables and a lower bound is computed using the new Lyapunov function computed in the previous iteration. The  $V$ - $s$  iteration continues as long as the lower bound continues to increase. In this iteration, Lyapunov functions are allowed to be of higher polynomial degree. Increasing the degree of the Lyapunov function will improve the lower bound at the expense of computational complexity. The computational time grows very rapidly with the degree of the Lyapunov function and so degree 4 candidates are about the maximum which can be used for problems like the GTM analysis.  $\underline{\beta}_2$  and  $\underline{\beta}_4$  will denote the best lower bounds computed with the  $V$ - $s$  iteration for quadratic and quartic Lyapunov functions. Nonlinear analysis code based on SOS optimization (including demos of the V-S iteration) can be downloaded from the URL<sup>31</sup>

### III. System Dynamics: Generic Transport Model (GTM) longitudinal dynamics

#### A. Polynomial model for GTM longitudinal dynamics

The familiar nonlinear equations of motion describing longitudinal dynamics of an aircraft given in Eq.14 contain high fidelity transcendental functions (trigonometric) and aerodynamic data as look up tables (LUT). The aerodynamic data is usually obtained through wind tunnel testing and flight tests and are not described as an analytical function of the states. In this section a procedure to obtain a pure polynomial approximation of the nonlinear GTM model is described. Simpler polynomial models are sometimes desirable for certain applications like, faster simulation or onboard real-time implementation as part of the flight control or vehicle health management algorithms. Similarly, polynomial nonlinear airplane dynamics model are required for nonlinear region of attraction (ROA) analysis, linear parameter varying (LPV) models, etc.

$$\dot{U} = \frac{1}{m}(F_x \cos\alpha + F_z \sin\alpha) \quad (14a)$$

$$\dot{\alpha} = \frac{1}{mU}(-F_x \sin\alpha + F_z \cos\alpha) + q \quad (14b)$$

$$\dot{\theta} = q \quad (14c)$$

$$\dot{q} = \frac{M_y}{I_{yy}} \quad (14d)$$

### 1. Trigonometric functions approximation

The trigonometric functions appearing in Eqs.14 can be conveniently approximated by third order Taylor series expansion, with reasonable accuracy, for example up to 45 degrees approximation error in sine and cosine is 0.35% and 2.2%, respectively (see Fig.1).

$$\sin(x) = x - \frac{1}{6}x^3 \quad (15a)$$

$$\cos(x) = 1 - \frac{1}{2}x^2 \quad (15b)$$

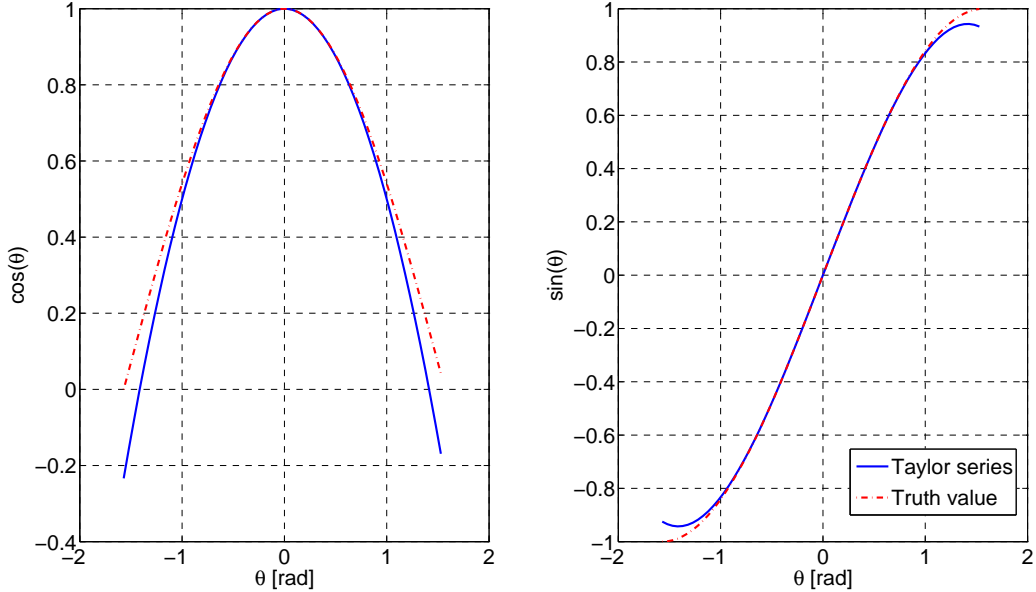


**Figure 1.** Trigonometric function approximations with Taylor series

### 2. Polynomial approximation of aerodynamic data

The aerodynamic data of GTM model is provided by NASA as look up tables (LUT). The LUT approach is widely used and is the most accurate way to capture the aerodynamic forces and moments at high angles of attack and sideslip,<sup>32,33</sup> which are difficult if not impossible to capture using analytic expressions. To obtain a good polynomial fit to the data the fitting process is restricted to a limited range of aerodynamic angles. The polynomial model described below is restricted to an angle of attack range of [0, 20] degrees, sideslip

$[-10, +10]$  degrees, and  $[-20, +20]$  degrees for derivatives with respect to control surface deflection, pitch rate.

Aerodynamic forces and moment enter the equations of motion as forcing function in the differential equations given in Eqs.14 through the following terms,

$$F_x = \bar{q}S_{ref}[C_x(\alpha) + C_x(\alpha, \delta_e) + C_x(\alpha, \hat{q})] + 2T_X(\delta_{th}) - mg\sin\theta \quad (16a)$$

$$F_z = \bar{q}S_{ref}[C_z(\alpha) + C_z(\alpha, \delta_e) + C_z(\alpha, \hat{q})] + 2T_Z(\delta_{th}) + mg\cos\theta \quad (16b)$$

$$M_y = \bar{q}S_{ref}\bar{c}[C_m(\alpha) + C_m(\alpha, \delta_e) + C_m(\alpha, \hat{q})] + 2\Delta Z_{ENG}T_X(\delta_{th}) \quad (16c)$$

where the aerodynamic coefficients of angle of attack,  $\alpha$ , pitch rate,  $q$ , and elevator deflection,  $\delta_e$ , are computed as LUTs in the full nonlinear simulation. The aim is to replace the LUTs with polynomial approximations using weighted least squares fit as discussed above. The polynomial approximation of the aerodynamic data is given in Table.1 in the Appendix.

### 3. Engine thrust polynomial model

In Eqs.14 it may be noted that engine thrust terms ( $T_X, T_Z$ ) are prefixed by multiple 2. This factor accounts for the two GTM engines, one on the port side and one on the starboard side. Equal thrust setting for both engines is assumed. The polynomial approximation of thrust as a function of throttle position is given by,

$$T(\delta_{th}) = (1.04 + 8.871\delta_{th}^2 + 9.151\delta_{th})^a \quad (17)$$

### The direction cosine vector

The engines are inclined with respect to the vehicle body axis, hence the thrust parameter given in the table must be transformed into body axes by a transformation vector, called a direction cosine vector (DCV). Although the transformation vector is composed of trigonometric functions, the engine alignment is fixed with respect to time, hence the DCV can be precomputed and used as a scaling vector on the engine axis thrust. Therefore no approximation of sines and cosines is necessary here. The reader is referred to the GTM Simulink model,<sup>33</sup> for more details on the transformation vector computation.

$$\begin{bmatrix} T_X \\ T_Y \\ T_Z \end{bmatrix} = [DCV]_{3 \times 1} T(\delta_{th}) \quad (18)$$

### 4. Airspeed inverse approximation

One potential problem arises in Eq.14(b) which has equivalent airspeed (EAS) in the denominator. A polynomial model for the dynamics should not include any rational terms. One way to avoid the rational dependence on EAS is to use a second order least squares polynomial fit over an EAS range of interest. This approach works well as seen in Fig.5. The nominal cruise EAS for GTM is 150 ft/s, hence the selected range is 100 ft/s to 300 ft/s to cover a wide flight envelope. The polynomial fitting for  $EAS^{-1}$  (written as  $U^{-1}$  for convenience) is given in Eq.19 below.

$$U^{-1} = 1.597336 \times 10^{-7}U^2 - 9.3590326 \times 10^{-5}U + 0.01729046705 \quad (19)$$

### 5. Aerodata/Engine data comparative plots: Lookup tables vs Polyfit

In Fig.2, 3 and 4, the true aerodynamic lookup table data for longitudinal forces and moment coefficients are compared with their polynomial approximations as described in Table.1. Fig.2 shows comparison of normalized pitchrate ( $\hat{q}$ ) derivatives. Fig.3 shows the comparison of angle of attack aero coefficients. Fig.4 presents a comparison of elevator control aerodynamic coefficients. The aim is to show that the polynomial

---

<sup>a</sup>For one P-70 engine only

models obtained for aerodynamic data are sufficiently accurate to capture aerodynamic characteristics of the airframe. Fig.4 also includes the comparison of engine thrust data with the polynomial approximation given in Eq.16a. In Fig.4 it may be noted that the X force coefficient ( $C_X$ ) due to elevator has been approximated to zero. This approximation is performed for two reasons. First, the magnitude of X-force coefficient is very small compared to Z-force coefficient. Secondly, the  $C_{x\delta_e}$  derivative is highly nonlinear and its not possible to capture the data with a low order fit. Since the magnitude of  $C_{x\delta_e}$  derivative is very small in comparison to  $C_{x\alpha}$  derivative, making it zero does not affect the dynamics by any significant measure.

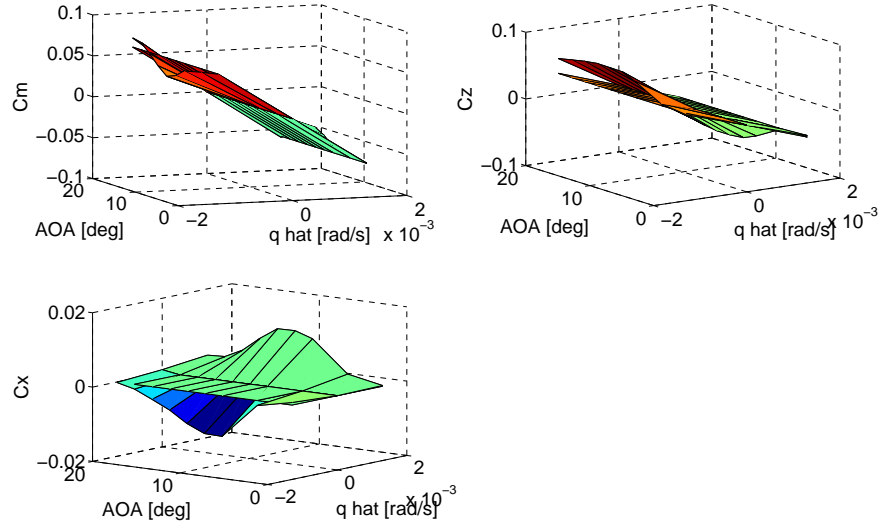


**Figure 2. Pitch rate aerodynamic derivate: polyfit vs LUT aerodata**

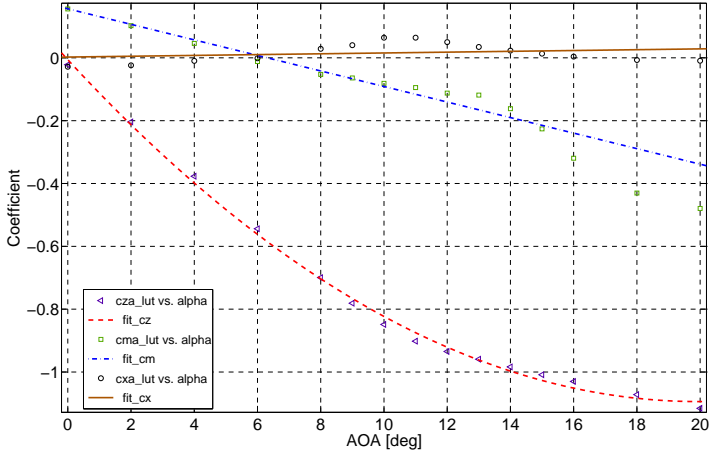


**Figure 3. Polynomial fitting of angle-of-attack aerodynamics derivate**

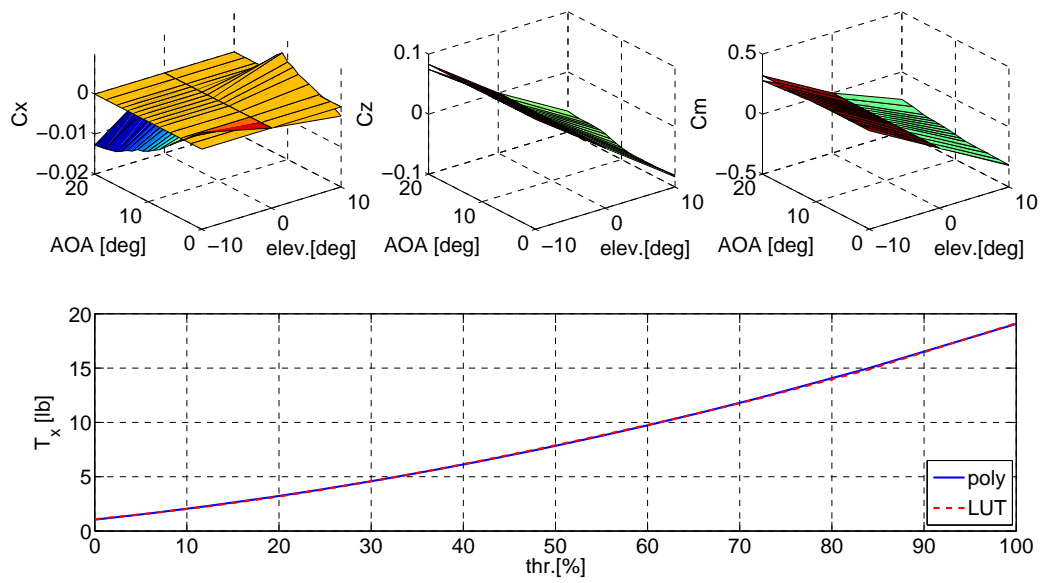


**Figure 4.** Control aeroderivatives: polyfit vs LUT aerodata

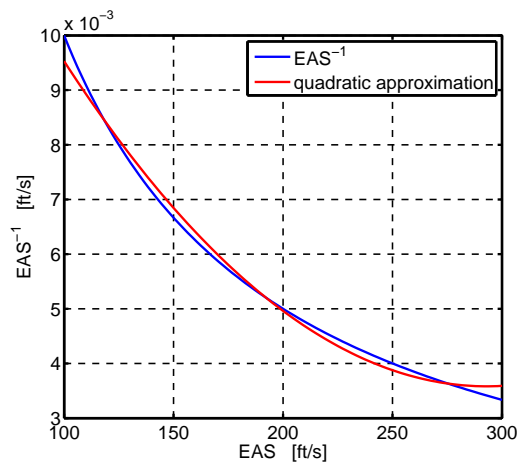


**Figure 5.** EAS inverse approximation

## 6. Polynomial equations of longitudinal motion

Finally, combining all polynomial approximations from previous sections and neglecting any monomials of degree greater than five, the polynomial longitudinal equations of motions are obtained by rewriting Eqs.14 as follows,

$$\begin{aligned}\dot{U} = & -0.071796\alpha^3\delta_{th}^2 + 0.032482\alpha^3U^2 + 2.6812\alpha^3\theta^2 - 2.6812\alpha^2\theta^3 - 0.074062\alpha^3\delta_{th} - 5.7479\alpha^2\delta_{th}^2 \\ & - 0.034453\alpha^2 * eas^2 - 0.002162\alpha\delta_e U^2 - 3.2851 \times 10^{-4}\alpha U^2 * q - 5.3708\alpha^3 - 5.9293\alpha^2\delta_{th} \\ & + 16.087\alpha^2\theta + 0.43077\alpha\delta_{th}^2 + 0.0033397\alpha U^2 - 16.087\alpha\theta^2 + 5.3623\theta^3 - 0.67386\alpha^2 + 0.44437\alpha\delta_{th} \\ & + 11.4958\delta_{th}^2 - 1.8821 \times 10^{-4}U^2 + 32.2246\alpha + 11.8586\delta_{th} - 32.174\theta + 1.3477\end{aligned}\tag{20a}$$

$$\begin{aligned}\dot{\alpha} = & 0.040619\alpha^3\delta_{th}^2 - 2.8888 \times 10^{-4}\alpha^3\delta_{th}U + 3.4371 \times 10^{-4}\alpha^3U^2 + 7.8376 \times 10^{-4}\alpha^3U\theta \\ & + 2.2917 \times 10^{-5}\alpha^2\delta_e U^2 + 3.1481 \times 10^{-5}\alpha^2\delta_{th}^2U - 7.2895 \times 10^{-8}\alpha^2\delta_{th}U^2 - 5.8362 \times 10^{-6}\alpha^2U^3 \\ & + 3.4823 \times 10^{-6}\alpha^2U^2q - 0.0011756\alpha^2U\theta^2 - 3.7716 \times 10^{-6}\alpha\delta_{th}^2U^2 - 9.3472 \times 10^{-9}\alpha U^4 \\ & + 7.8376 \times 10^{-4}\alpha U\theta^3 - 7.093 \times 10^{-10}\delta_e U^4 - 1.0778 \times 10^{-10}U^4q + 0.041901\alpha^3\delta_{th} \\ & - 3.283 \times 10^{-5}\alpha^3U - 0.11368\alpha^3\theta - 0.0045663\alpha^2\delta_{th}^2 + 3.2475 \times 10^{-5}\alpha^2\delta_{th}U + 8.4125 \times 10^{-4}\alpha^2U^2 \\ & + 0.17053\alpha^2\theta^2 + 0.0016802\alpha\delta_{th}^2U - 3.8906 \times 10^{-6}\alpha\delta_{th}U^2 + 4.1641 \times 10^{-6}\alpha U^3 + 1.0556 \times 10^{-5}\alpha U^2\theta \\ & - 0.11368\alpha\theta^3 + 3.1599 \times 10^{-7}\delta_e U^3 + 1.4133 \times 10^{-7}\delta_{th}^2U^2 - 6.7118 \times 10^{-12}U^4 + 4.8015 \times 10^{-8}U^3q \\ & - 5.2779 \times 10^{-6}U^2\theta^2 + 0.004762\alpha^3 - 0.0047104\alpha^2\delta_{th} + 0.002355\alpha^2U - 0.24372\alpha\delta_{th}^2 + 0.0017333\alpha\delta_{th}U \\ & - 6.0445 \times 10^{-4}\alpha U^2 - 0.0047026\alpha U\theta - 4.5834 \times 10^{-5}\delta U^2 - 6.2962 \times 10^{-5}\delta_{th}^2U + 1.4579 \times 10^{-7}\delta_{th}U^2 \\ & + 2.9901 \times 10^{-9}U^3 - 6.9645 \times 10^{-6}U^2q + 0.0023513U\theta^2 - 0.34159\alpha^2 - 0.25141\alpha\delta_{th} + 1.9698 \times 10^{-4}\alpha U \\ & + 0.6821\alpha\theta + 0.0091326\delta_{th}^2 - 6.4949\delta_{th}U + 1.0139 \times 10^{-5}U^2 - 0.34105\theta^2 - 0.028572\alpha + 0.0094208\delta_{th} \\ & - 0.0047099U + q + 0.68317\end{aligned}\tag{20b}$$

$$\begin{aligned}\dot{q} = & -0.030927\alpha^3U^2 + 0.01089\alpha^2U^2 - 0.003\alpha U^2 - 0.002765\delta_e U^2 - 2.0431 \times 10^{-4}U^2q + 1.2398\delta_{th}^2 \\ & + 2.3418 \times 10^{-4}U^2 + 1.2789\delta_{th} + 0.14535\end{aligned}\tag{20c}$$

$$\dot{\theta} = q\tag{20d}$$

## 7. Comparison with full nonlinear simulation

The simulation response to an elevator perturbation using the polynomial equations derived in Eqs.17(a)-(d), is compared with the full nonlinear GTM simulation model. Fig.6 shows the comparative plots. In this example, the two GTM models, full nonlinear and the polynomial model described in this report are first trimmed to a straight and level flight at EAS= 90knots. At time t= 1 second the elevator channel is perturbed with a pulse input lasting two seconds. The response of the airplane is captured through the longitudinal states, namely, equivalent airspeed (EAS), pitch rate (q), angle of attack ( $\alpha$ ), and pitch attitude ( $\theta$ ). The throttle is kept constant at its trim setting through out the maneuver. It is observed that the response of polynomial model closely matches the full nonlinear GTM model, as desired.

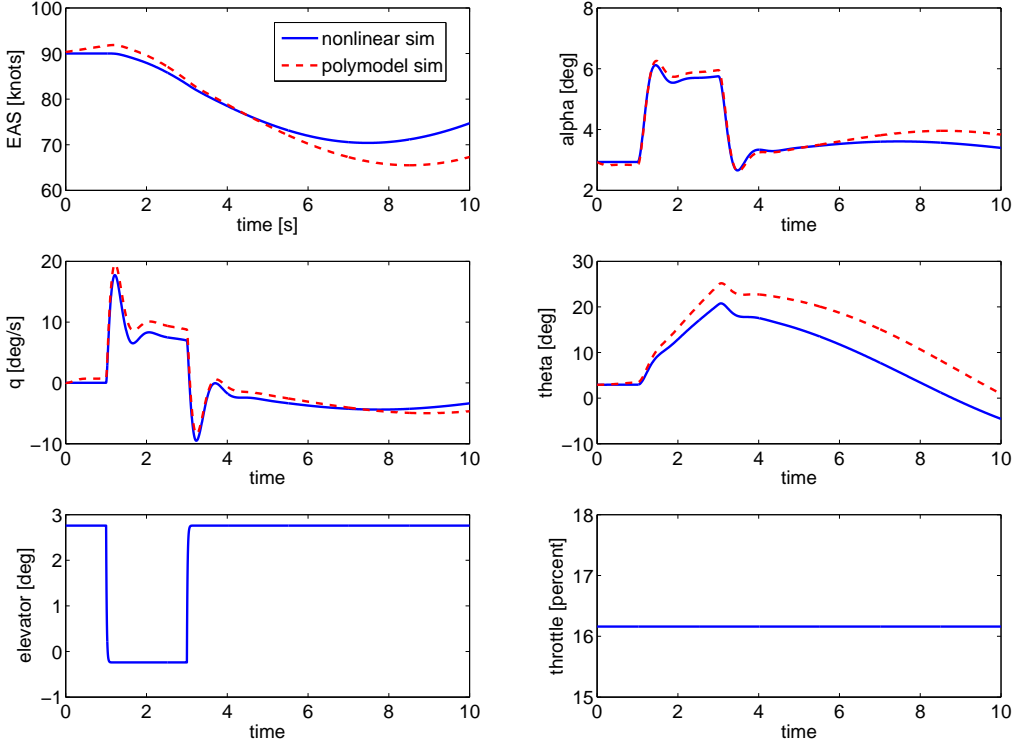


**Figure 6.** Time response comparison: Full nonlinear GTM model vs Polynomial EOMs

### B. Closed loop model GTM model: Pitch command tracking

A simple Proportional-Integral (PI) controller for pitch attitude tracking is presented and the polynomial model for the closed-loop system is derived. In a later section the closed-loop GTM model will be analyzed alongside the open-loop model for the regions of attraction. The controller block diagram is shown in Fig.7. The input to the controller is the pitch attitude tracking error and controller output is elevator command. Throttle control is not used in the closed loop, hence is kept fixed at its trim value for all analysis and simulation, unless specified.

The presence of the integrator in the controller introduces an additional state into the system in place of the elevator input. Assuming a constant pitch reference command, the elevator state derivative can be obtained using control law described in Fig.7 as,

$$\dot{\delta}_e = -20\varepsilon(5(\theta_{ref} - \theta) - \dot{\theta}) \quad (21)$$

where,  $\dot{\theta}$  is obtained from GTM polynomial dynamics, pitch state derivative in Eq.6(d). Substituting for the elevator state derivative, the new closed-loop state-space in  $\mathbb{R}^5$  is obtained. To avoid repetition, the full closed-loop polynomial equations are not presented, but the same may be obtained easily by combining Eq.B with Eqs.6. In Fig.8 the closed loop response to a step input is presented, with initial conditions at straight and level flight at EAS= 150 m/s or 90 knots.

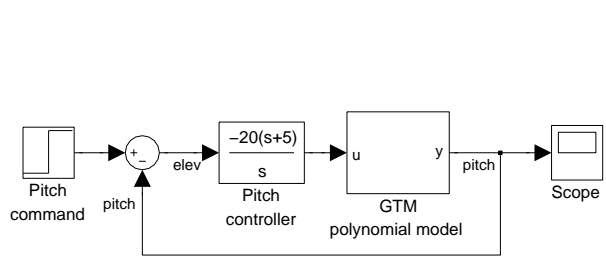


Figure 7. GTM closed loop interconnection block diagram with pitch tracking controller

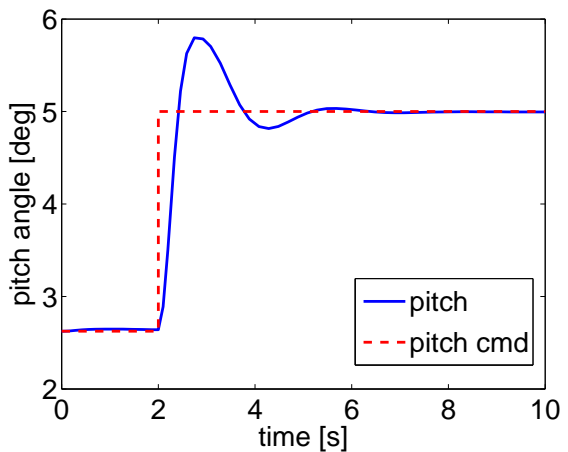


Figure 8. Nominal step response of the closed loop GTM polynomial model

## IV. Results

### A. Reachable Sets analysis

The polynomial model derived in Eq.6 is trimmed for straight and level flight at EAS= 150ft/s or 90 knots. The EAS is independent of altitude, hence trim altitude is not relevant. The longitudinal axis GTM polynomial model is linearized around this trim point resulting in a fourth order system with two input, elevator and throttle. For the purpose of analysis we will only consider elevator input, keeping throttle at its trimmed value. Peak input constraint on elevator is kept to 20degrees magnitude.

Based on the theory presented in section.II.A the LMI optimization problem is setup for computing reachable set with peak-input constraint, Eq.19 and the reachable set with unit-input energy constraint, Eq.17. Fig.9 shows the two reachable sets obtained around trim states. The reachable set with unit-input energy constraint,  $\mathcal{R}_{ue}$  is smaller of the two and is contained within the reachable set for unit-peak input constraint. This is expected as peak input is not constrained by energy bound and can exert more control energy on the states. Its interesting to note that the ellipsoid stretched by different amount along each coordinate. Larger dimension in a particular direction implies that state is more controllable.

It is important to highlight some of the limitations of reachability analysis. By definition reachability applies to linear systems, but by applying peak inputs or large perturbations the system can be driven far away from where the linear model is valid. One approach to address this is to incorporate LPV model instead. Secondly, reachability of a state is not related to the ability to trim at a given state. In practice, it can be expected that *trimmable set* is a proper subset of the reachable set. But reachable set does not indicate where this boundary might lie. Thirdly, reachable set computation as described in the section.II.A, implicitly assumes reachability over infinite time horizon, which is of little practical importance. However, it is also understood that the linear system would settle to a steady state governed by the maximum settling time of its modes. Hence, bounds on the reach time can be established in practice. Despite these limitations, reachability analysis points in the right direction towards which states may be more controllable, and hence can be important from flight safety perspective. Reachability analysis also allows actuator dynamics to be included in the analysis including hard limits on control authority. Inclusion of damage scenarios is also a simple task by making appropriate changes to the A and B matrices.

### B. Region-of-Attraction analysis

The region of attraction of the open-loop GTM polynomial model is estimated about the identical trim condition as before, EAS = 150 ft/sec and steady/level flight (flight path angle = 0 deg). The state and

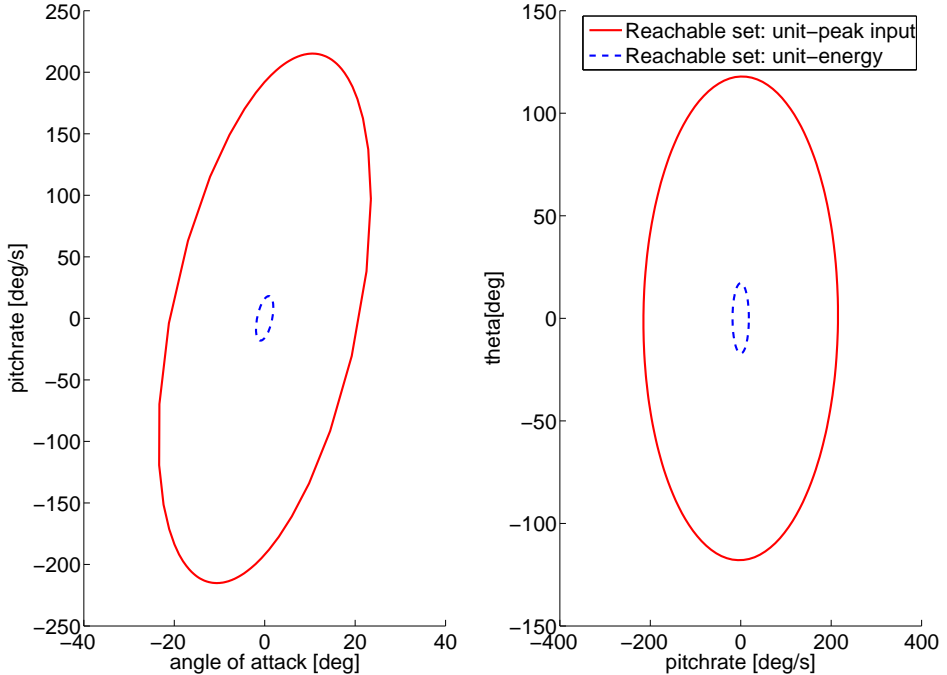


**Figure 9. Reachable sets with unit-energy constraint and unit-peak input constraint for Linear GTM model trimmed at EAS=150ft/s, straight and level**

input for this trim condition are:

$$\begin{aligned}
 U &= 150 \text{ ft/sec} \\
 \alpha &= 0.0458 \text{ rads} = 2.62 \text{ degs} \\
 q &= 0 \text{ rads/sec} = 0 \text{ degs/sec} \\
 \theta &= 0.0458 \text{ rads} = 2.62 \text{ degs} \\
 \delta_{thr} &= 0.0859 \text{ (Normalized)} \\
 \delta_e &= 0.0463 \text{ rads} = 2.66 \text{ degs}
 \end{aligned}$$

To improve the numerical conditioning, the states are shifted and scaled using the scaling matrix  $D$ :  $z := D^{-1}(x - x_{trim})$  where:

$$D := \text{diag}(50\text{ft/sec}, 20\text{deg}, 50\text{deg/sec}, 20\text{deg})$$

The shape function is defined to be  $p(z) := z^T z$ . This is an ellipsoid in the original coordinates with radii along each coordinate given by the entries of  $D$ . All results were generated on a 2.66 GHz Intel Core 2 Quad processor PC.

First, a Monte Carlo search is run to find the smallest value of  $p(z)$  resulting in a divergent trajectory. After 10000 simulations, the smallest value of  $p(z)$  was  $\beta_{MC} = 3.13$ .  $\beta_{MC}$  is an upper bound on the largest ellipsoid in the region of attraction. It took 1721 sec  $\approx$  29min to run these 10000 simulations. The initial condition leading to a divergent trajectory was:

$$\begin{aligned}
 U &= 186.12 \text{ ft/sec} \\
 \alpha &= -0.41 \text{ rads} = -23.48 \text{ degs} \\
 q &= 0.008 \text{ rads/sec} = 0.45 \text{ degs/sec} \\
 \theta &= 0.38 \text{ rads} = 21.66 \text{ degs}
 \end{aligned}$$

The divergent trajectory starting from this initial condition is shown in Figure 10. The EAS goes to zero around  $t = 6$  sec and so the polynomial model is not valid for the entire simulation.

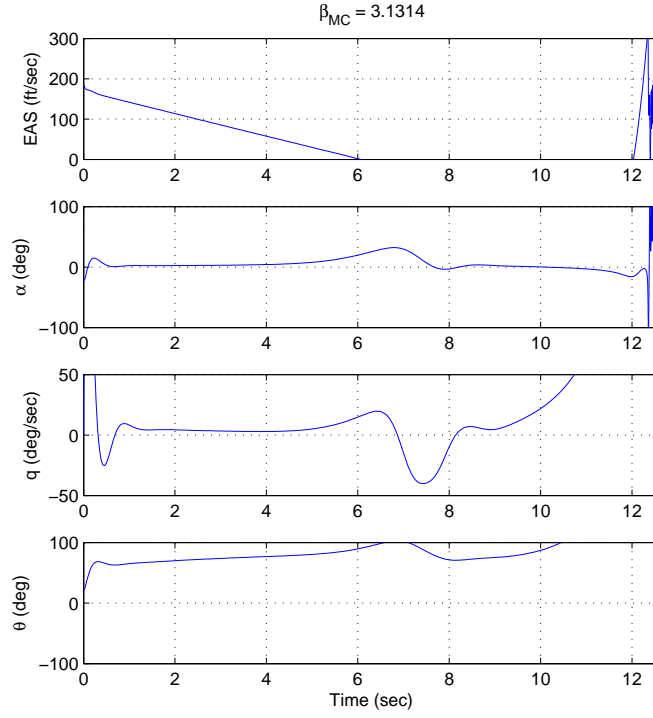


**Figure 10. Divergent Trajectory from Monte Carlo Simulations**

Next, SOS optimization is used to find the largest value of  $p(z)$  that is provably in the region of attraction. The provable region using the quadratic Lyapunov function from linear analysis was only  $\beta_{LIN} = 1.89 \times 10^{-5}$ . This took 20.9 sec. Running one hundred steps of the V-s iteration with quartic Lyapunov functions increased the provable region to  $\beta_4 = 1.87$ . This took 7074.8 sec  $\approx 117.9$  min. The progress of the V-s iteration with quartic Lyapunov functions for the open loop case is shown in Figure 13. This figure also shows the progress of Monte Carlo search for divergent trajectory as a function of the number of simulations.  $\beta_{MC}$  decreased rapidly in the first 300 simulations and then made only small progress thereafter, as it gets harder and harder to find an divergent initial condition as one moves closer to the equilibrium states.

The inner/outer bounds on the region of attraction can be visualized by plotting slices of the ellipsoid  $p(z) = \beta$ . Figure 15 shows a slice in the AOA-pitchrate plane along with that of the closed loop ROA analysis. All curves are drawn in the original coordinates with respect to the trim condition. The region of attraction cannot contain all of this ellipsoid since we found a divergent trajectory on the surface of this ellipsoid. Every initial condition of these ellipsoids was proven, via the SOS methods, to be in the region of attraction. Increasing the degree of the Lyapunov function enables the SOS optimization to prove a larger estimate of the region of attraction. It is possible that a degree 6 Lyapunov function could prove an even larger region but this would require significantly more computation time. Figure 16 shows another slice of the ellipsoid in the EAS-pitch plane.

These ROA analysis results indicate that in the EAS/ $\alpha$  and  $\theta/\alpha$  planes the open-loop aircraft will return to the trim solution:  $U = 150$  ft/sec,  $\alpha = 2.62^\circ$ ,  $q = 0^\circ/\text{sec}$ , and  $\theta = 2.62^\circ$  for initial perturbations in an ellipse defined by  $U$  between 80 and 220 ft/sec,  $\theta$  and  $\alpha$  perturbations between  $-24^\circ$  and  $30^\circ$ .

Comparing ROA bounds for open loop GTM model with the closed loop model, we find from Fig.14 that provable stable region with SOS methods is larger for the closed loop case.  $\beta$  lower bound for the open loop case was found to be 1.87 while with the pitch controller wrapped around  $\beta$  was found to be 2.16.

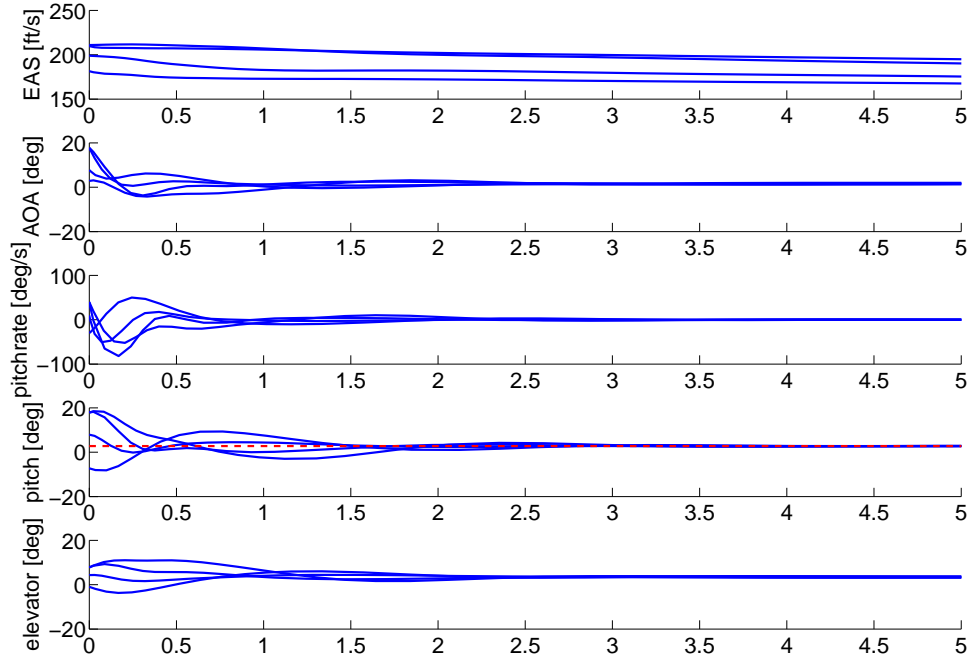


Figure 11. Stable convergent trajectories with initial conditions on the surface of the ellipsoid with proven stability,  $\beta = 2.16$ . Closed loop polynomial GTM model, elevator saturation included [ $\pm 20$  deg].

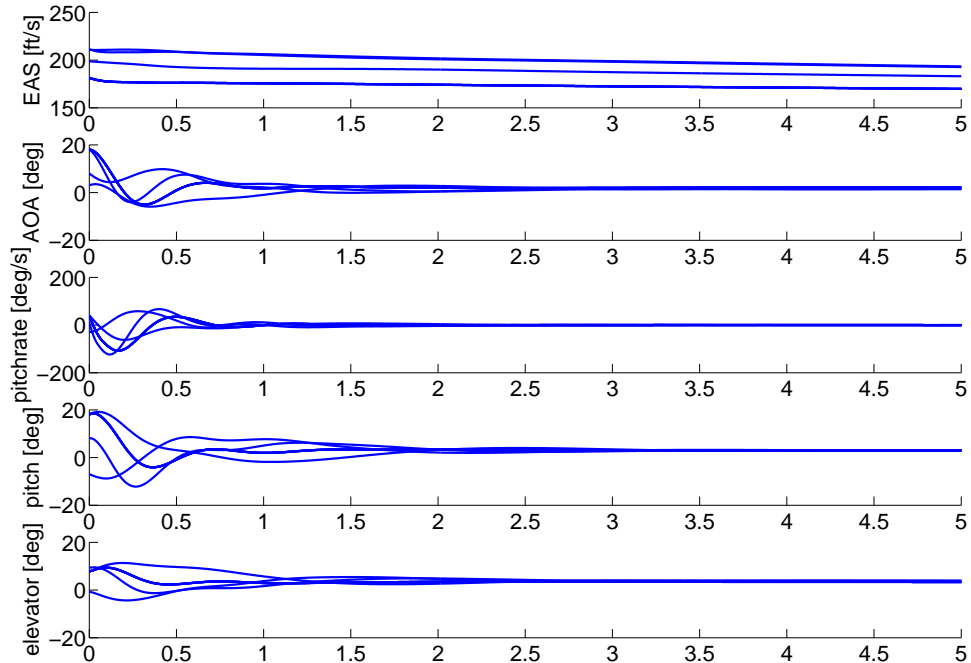


Figure 12. Full nonlinear closed loop GTM model simulation with initial conditions on proven ellipsoid boundary,  $\beta = 2.16$ .

This indicates that presence of a well designed feedback controller actually enhances the ROA for a system like GTM. Corresponding to the  $\beta$  bound for the closed loop system, ROA ellipsoid projections are given alongwith that of the open loop case, in Figs.15,16. It may be noted that upper bound for  $\beta$  computed using Monte Carlo simulation does not show the same trend. Its due to the stochastic nature of Monte Carlo sim and much larger number of iterations must be performed to arrive to a high confidence bound. Unfortunately, this is computationally intensive. Figs.15,16 also show rectangular boundaries to indicate the region of state-space for which the derived polynomial dynamics model is valid. This is to show that any results or claims lying outside the boundary are not valid strictly speaking. A solution maybe to find ways to extend the validity of the model, which in certain cases can be difficult while keeping degree of the polynomial model tractably small from numerical computation point of view.

In the Fig.11 simulation results for the closed loop GTM polynomial model is presented on which ROA analysis was carried out. elevator position constraints of  $\pm 20$  degrees was also included. Initial conditions for the five states, including elevator state was chosen randomly on the surface for which guaranteed stability boundary was established as  $\beta = 2.16$  in this section, also shown graphically in Figs.14, 15 and 16. It can be seen that the all initial conditions converge to the trim point as predicted by the analysis. In Fig.12 the same initial conditions are simulated in the full nonlinear GTM simulation model<sup>33</sup> with the same controller as described previously. Again, we find that the trajectories converge to the trim. Its worth noting that in the particular simulation instances the elevator limits were never exceeded so the effect of control constraints was not evident. It is entirely possible for any other dynamical system or a different control law that the control authority limits may be exceeded, the ROA analysis does not take that into account and may result in unstable trajectories despite of being proven otherwise. This may be seen as a limitation of the current approach.

The main limitation of ROA methods is the computational requirements and the fact that complexity of the problem scales badly with increase in dimensions of the system. At present efforts are also being applied to be able to include actuator nonlinearities and hard limits in the ROA analysis, which is missing so far.

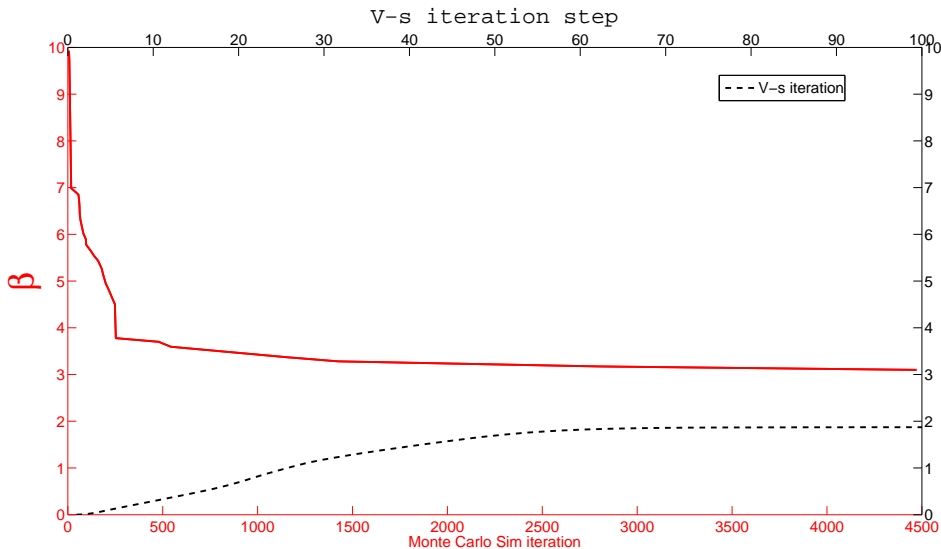


Figure 13. ROA bounds estimate, open loop GTM model

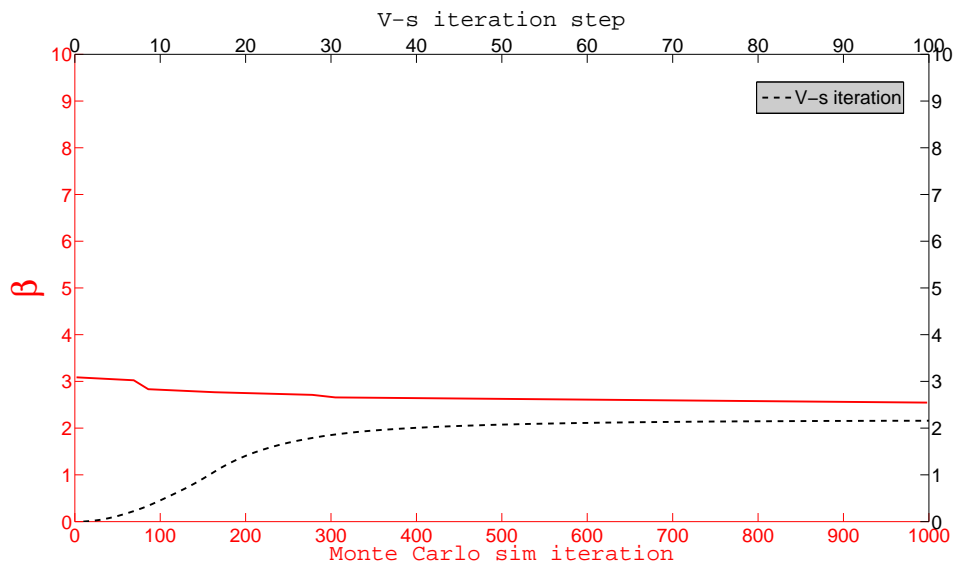


Figure 14. ROA bounds estimate, closed loop GTM model

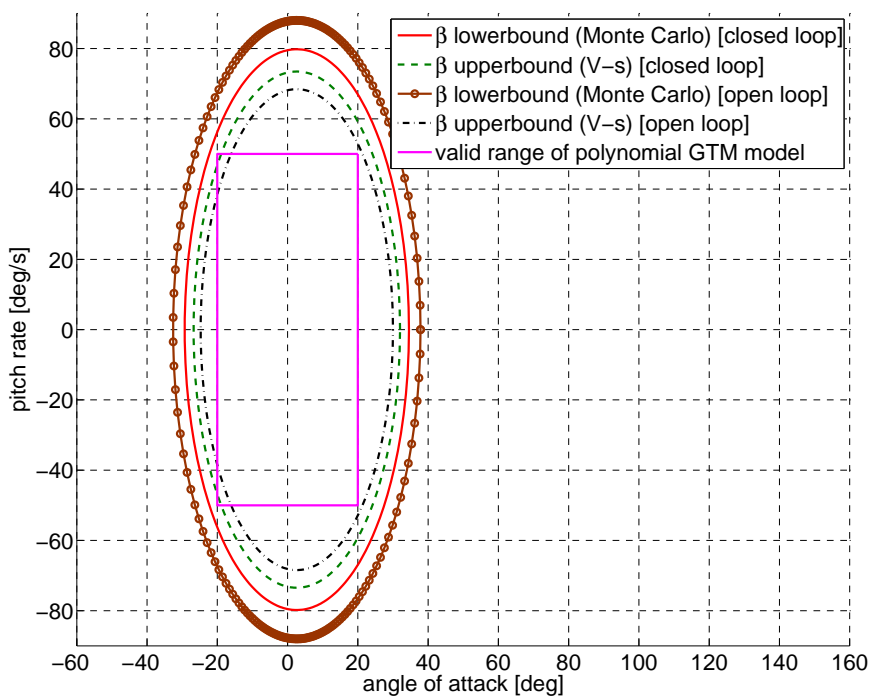


Figure 15. ROA ellipsoids comparison: open loop vs closed loop. Projected in AOA,pitchrate plane

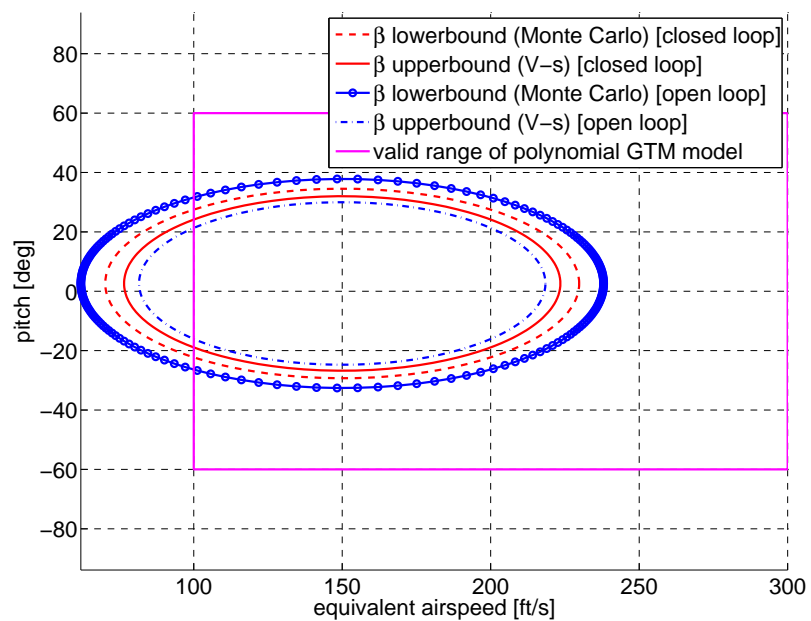


Figure 16. ROA ellipsoids comparison: open loop vs closed loop. Projected in EAS,pitch angle plane

## V. Summary

The two fundamentally different approaches to the problem of dynamic flight envelope assessment have been applied to the GTM airplane model. Assessment of the region of attraction around a chosen trim and the linear reachable set under input constraint was derived computationally and validated using time domain simulation using the full nonlinear model. Limitations and merit of each approach was discussed briefly and points to the future direction for research.

## Appendix

**Table 1. Polynomial approximation coefficients for the aerodata**

Coefficient	Polynomial approximation
$C_x(\alpha)$	$a_{11}\alpha + a_{01} = 0.001302\varepsilon\alpha + 0.002515$
$C_z(\alpha)$	$a_{22}\alpha^2 + a_{12}\alpha + a_{02} = 0.002731\varepsilon^2\alpha^2 - 0.109\varepsilon\alpha - 0.005959$
$C_m(\alpha)$	$a_{13}\alpha + a_{03} = -0.02511\varepsilon\alpha + 0.1506$
$C_x(\alpha, \hat{q})$	$C_{x_q}q = 0.0q$
$C_z(\alpha, \hat{q})$	$C_{z_q}q = -24\frac{\bar{c}}{2U}q$
$C_m(\alpha, \hat{q})$	$C_{m_q}q = -45\frac{\bar{c}}{2U}q$
$C_x(\alpha, \delta_e)$	$C_{x_{\delta_e}}\delta_e = 0.0\varepsilon\delta_e$
$C_z(\alpha, \delta_e)$	$C_{z_{\delta_e}}\delta_e = -0.0083\varepsilon\delta_e$
$C_m(\alpha, \delta_e)$	$C_{m_{\delta_e}}\delta_e = -0.032\varepsilon\delta_e$

## References

- <sup>1</sup>Shin, J., "The NASA aviation safety program-An overview," *ASME TURBO EXPO, Munich, Germany*, May.
- <sup>2</sup>Shin, J.-Y., "Analysis of linear parameter varying system models based on reachable sets," CR 211231, ICASE, NASA Langley Research Center, 2001.
- <sup>3</sup>Cross, E. A. and Mitchell, I. M., "Level set methods for computing reachable sets of systems with differential algebraic equation dynamics," *American Control Conference, Seattle, Washington, USA*, 2008.
- <sup>4</sup>Alexandre M. Bayen, Ian M. Mitchell, M. M. O. and Tomlin, C. J., "Aircraft autolander safety analysis through optimal control-based reach set computation," *Journal of Guidance, Control and Dynamics*, Vol. 30, No. 1, 2007.
- <sup>5</sup>Tibken, B., "Estimation of the domain of attraction for polynomial systems via LMIs," *Proceedings of the IEEE Conference on Decision and Control*, 2000, pp. 3860–3864.
- <sup>6</sup>Tibken, B. and Fan, Y., "Computing the domain of attraction for polynomial systems via BMI optimization methods," *Proceedings of the American Control Conference*, 2006, pp. 117–122.
- <sup>7</sup>Hachicho, O. and Tibken, B., "Estimating domains of attraction of a class of nonlinear dynamical systems with LMI methods based on the theory of moments," *Proceedings of the IEEE Conference on Decision and Control*, 2002, pp. 3150–3155.
- <sup>8</sup>Topcu, U., Packard, A., and Seiler, P., "Local stability analysis using simulations and sum-of-squares programming," *Automatica*, Vol. 44, No. 10, 2008, pp. 2669–2675.
- <sup>9</sup>Tan, W., *Nonlinear Control Analysis and Synthesis using Sum-of-Squares Programming*, Ph.D. thesis, University of California, Berkeley, 2006.
- <sup>10</sup>Kailath, T., *Linear Systems*, Prentice Hall Information and System Sciences Series, 1980.
- <sup>11</sup>S. Boyd, L. El Ghaoui, E. F. and Balakrishnan, V., *Linear Matrix Inequalities in System and Control Theory*, SIAM, 1994.
- <sup>12</sup>F.Zheng, Q.-G. W. and T.H.Lee, "A parameter optimization approach to solving Quasi-LMI problems," *Proc. 40th IEEE Conf. on Decision and Control*, 2001, pp. 3607–3612.
- <sup>13</sup>Khalil, H., *Nonlinear Systems*, Prentice Hall, 3rd ed., 2002.
- <sup>14</sup>Vidyasagar, M., *Nonlinear Systems Analysis*, Prentice Hall, 2nd ed., 1993.
- <sup>15</sup>Parrilo, P., *Structured Semidefinite Programs and Semialgebraic Geometry Methods in Robustness and Optimization*, Ph.D. thesis, California Institute of Technology, 2000.
- <sup>16</sup>Vannelli, A. and Vidyasagar, M., "Maximal Lyapunov functions and domains of attraction for autonomous nonlinear systems," *Automatica*, Vol. 21, No. 1, 1985, pp. 69–80.
- <sup>17</sup>Hauser, J. and Lai, M., "Estimating quadratic stability domains by nonsmooth optimization," *Proceedings of the American Control Conference*, 1992, pp. 571–576.

- <sup>18</sup>Genesio, R., Tartaglia, M., and Vicino, A., "On the estimation of asymptotic stability regions: State of the art and new proposals," *IEEE Transactions on Automatic Control*, Vol. 30, No. 8, 1985, pp. 747–755.
- <sup>19</sup>Davison, E. and Kurak, E., "A computational method for determining quadratic Lyapunov functions for nonlinear systems," *Automatica*, Vol. 7, 1971, pp. 627–636.
- <sup>20</sup>Chiang, H.-D. and Thorp, J., "Stability regions of nonlinear dynamical systems: A constructive methodology," *IEEE Transactions on Automatic Control*, Vol. 34, No. 12, 1989, pp. 1229–1241.
- <sup>21</sup>Jarvis-Wloszek, Z., *Lyapunov Based Analysis and Controller Synthesis for Polynomial Systems using Sum-of-Squares Optimization*, Ph.D. thesis, University of California, Berkeley, 2003.
- <sup>22</sup>Jarvis-Wloszek, Z., Feeley, R., Tan, W., Sun, K., and Packard, A., "Some Controls Applications of Sum of Squares Programming," *Proceedings of the 42nd IEEE Conference on Decision and Control*, Vol. 5, 2003, pp. 4676–4681.
- <sup>23</sup>Tan, W. and Packard, A., "Searching for control Lyapunov functions using sums of squares programming," *42nd Annual Allerton Conference on Communications, Control and Computing*, 2004, pp. 210–219.
- <sup>24</sup>Jarvis-Wloszek, Z., Feeley, R., Tan, W., Sun, K., and Packard, A., *Positive Polynomials in Control*, Vol. 312 of *Lecture Notes in Control and Information Sciences*, chap. Controls Applications of Sum of Squares Programming, Springer-Verlag, 2005, pp. 3–22.
- <sup>25</sup>Tan, W., *Nonlinear Control Analysis and Synthesis using Sum-of-Squares Programming*, Ph.D. thesis, University of California, Berkeley, 2006.
- <sup>26</sup>Topcu, U., Packard, A., Seiler, P., and Wheeler, T., "Stability region analysis using simulations and sum-of-squares programming," *Proceedings of the American Control Conference*, 2007, pp. 6009–6014.
- <sup>27</sup>Topcu, U., *Quantitative Local Analysis of Nonlinear Systems*, Ph.D. thesis, University of California, Berkeley, 2008.
- <sup>28</sup>Prajna, S., Papachristodoulou, A., Seiler, P., and Parrilo, P. A., *SOSTOOLS: Sum of squares optimization toolbox for MATLAB*, 2004.
- <sup>29</sup>Lofberg, J., "YALMIP : A Toolbox for Modeling and Optimization in MATLAB," *Proceedings of the CACSD Conference*, Taipei, Taiwan, 2004.
- <sup>30</sup>Sturm, J., "Using SeDuMi 1.02, a MATLAB toolbox for optimization over symmetric cones," *Optimization Methods and Software*, 1999, pp. 625–653.
- <sup>31</sup>"ROA estimation, SOS Tools, etc." <http://jagger.me.berkeley.edu/software/acc09/>.
- <sup>32</sup>A.M.Murch, J., "Recent NASA research on aerodynamic modeling of post-stall and spin dynamics of large transport airplanes," *45th AIAA Aerospace Sciences Meeting and Exhibit, Reno, Nevada*, 2007.
- <sup>33</sup>Cox, D., "The GTM DesignSim v0905," .
- <sup>34</sup>Stevens, B. L. and Lewis, F. L., *Aircraft Control and Simulation*, Wiley Interscience, 2nd Edition, 2003.